

BlindDiff: Empowering Degradation Modelling in Diffusion Models for Blind Image Super-Resolution

Feng Li¹ Yixuan Wu² Zichao Liang² Runmin Cong³ Huihui Bai^{2,†} Yao Zhao² Meng Wang¹
¹Hefei University of Technology ²Beijing Jiaotong University ³Shandong University

Abstract

Diffusion models (DM) have achieved remarkable promise in image super-resolution (SR). However, most of them are tailored to solving non-blind inverse problems with fixed known degradation settings, limiting their adaptability to real-world applications that involve complex unknown degradations. In this work, we propose *BlindDiff*, a DM-based blind SR method to tackle the blind degradation settings in SISR. *BlindDiff* seamlessly integrates the MAP-based optimization into DMs, which constructs a joint distribution of the low-resolution (LR) observation, high-resolution (HR) data, and degradation kernels for the data and kernel priors, and solves the blind SR problem by unfolding MAP approach along with the reverse process. Unlike most DMs, *BlindDiff* firstly presents a modulated conditional transformer (MCFormer) that is pre-trained with noise and kernel constraints, further serving as a posterior sampler to provide both priors simultaneously. Then, we plug a simple yet effective kernel-aware gradient term between adjacent sampling iterations that guides the diffusion model to learn degradation consistency knowledge. This also enables to joint refine the degradation model as well as HR images by observing the previous denoised sample. With the MAP-based reverse diffusion process, we show that *BlindDiff* advocates alternate optimization for blur kernel estimation and HR image restoration in a mutual reinforcing manner. Experiments on both synthetic and real-world datasets show that *BlindDiff* achieves the state-of-the-art performance with significant model complexity reduction compared to recent DM-based methods. Code will be available at <https://github.com/lifengcs/BlindDiff>

1. Introduction

Single image super-resolution (SISR) is a long-standing problem in computer vision and image restoration, which has attracted significant attention due to its ill-posed nature and broad practical applications. SISR refers to generating a high-resolution (HR) image \hat{x} from a low-resolution (LR)

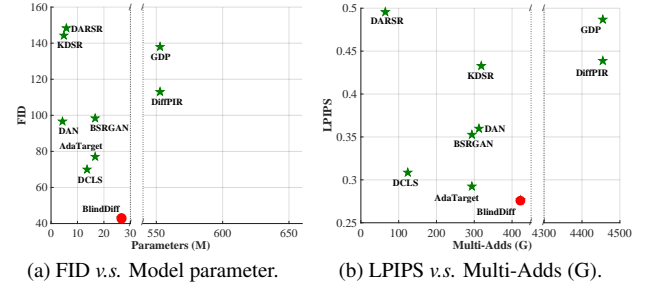


Figure 1. Our *BlindDiff* achieves the state-of-the-art performance for 4× blind SR (Table 2) which being more computational efficient than existing DM-based methods. The Multi-Adds are computed based on the LR size of 128 × 128.

observation y given through a degradation model

$$y = (k \otimes x) \downarrow_s + n \quad (1)$$

where k denotes the blur kernel convolved with x , followed by a downsampling operation with scale factor s . n is usually assumed as the additive white Gaussian noise (AWGN). Over the past years, methods for SISR have been dominated by deep learning approaches [4, 9, 14, 24, 39, 42, 51]. Most of them mainly work on pre-defined degradations (*e.g.* bicubic downsampling), which train powerful deep convolutional networks with end-to-end supervision on synthesized numerous LR-HR pairs. Despite their success, they would deteriorate in performance when applied to other unseen degradations. This is particularly evident in real world where the degradations are complicated and unavailable.

To overcome this limitation, recent researchers pay increasing attention to blind image super-resolution (SR) [1, 15, 22, 38], where their key steps lie in degradation estimation (mostly blur kernel k) and degradation-aware SR reconstruction. One option [1, 25] is to estimate the underlying k from LR input y and apply that to non-blind SR models [34, 48] for HR image generation. Another approach [13, 15, 27] is to unify kernel estimation and SR reconstruction in a single end-to-end framework. However, their results still suffer from noticeable artifacts and low perceptual quality in dealing with complex degradations.

Very recently, the emerging diffusion models (DM) [17, 35] have been demonstrated as a powerful generative model for high-fidelity image generation [10, 20, 31, 32]. Currently, there are two main paradigms of DM-based methods for SISR. One is to train the DM from scratch conditioned on LR images [23, 33]. The other more popular is to design problem-agnostic models [5, 7, 20, 41], which employs off-the-shelf pre-trained DMs as the generative prior for general-purpose restoration. Nevertheless, it is important to note that both approaches typically focus on non-blind inverse problems, meaning that the image degradation is assumed to be known and fixed. This is impractical in real-world applications, thereby severely restricting their generalization ability.

In this work, we explore the potential of DMs for blind SR and propose BlindDiff, a novel diffusion super-resolver that is flexible and robust to various degradations. This method is inspired by recent denoising diffusion probabilistic models (DDPM) [7, 17, 36] for non-blind inverse problems and extend them to the blind settings in SISR with significant modifications. To be specific, BlindDiff formulates the blind SR problem under a maximum a posteriori (MAP) framework and unfolds it along with the reverse process in DDPM. Following the MAP optimization paradigm, the key issue now boils down to acquiring the priors of HR clean data and degradation kernels with DDPM. In this case, directly applying conventional pre-trained DDPMs to provide generative priors is not appropriate as they lack the modelling of degradations. Hence, we reconfigure the denoising network and propose the modulated conditional transformer (MCFormer) trained with noise and kernel constraints to guarantee data and kernel priors in each posterior sampling procedure. We then treat the reverse diffusion process as a deep network and introduce a kernel-aware gradient term with respect to the LR condition and two priors, which guide the diffusion model to learn degradation consistency knowledge. Therefore, the denoised images and blur kernels can be jointly optimized by the gradients backpropagated from intermediate states. Besides, such a gradient term can bridge two adjacent iterations to form a closed loop for alternate kernel and HR image estimation until approaching their best approximations with the iteration going on. Moreover, MCFormer injects the modulation between extracted kernel knowledge and image features to exploit their interdependence so that can learn multi-level degradation-aware features for better generation. Attributed to the intrinsic incorporation of MAP-based solution, BlindDiff has highly intuitive physical meanings and is consistent with the classical degradation model (Eq. (1)), achieving excellent adaptation to various complex degradations in real applications.

The main contributions of this work are four-fold:

- We propose BlindDiff, an effective yet efficient diffu-

sion solver for blind SR. BlindDiff explicitly models the degradation kernels in SISR leveraging the power of DMs, which is expected to achieve high-fidelity generation in real scenarios.

- BlindDiff unfolds MAP approach in diffusion models, which enables iteratively alternate optimization for blur kernel estimation and HR image restoration along with the reverse process.
- A modulated conditional transformer (MCFormer) is proposed as the denoising network, which provides data and kernel priors for posterior sampling. Besides, MCFormer incorporates the kernel modulation mechanism to adjust image features in accordance with kernel information, facilitating the acquisition of multi-level degradation-aware prior features.
- Extensive experiments on both synthetic and real-world datasets show the SOTA performance of our method. Particularly, it surpasses existing DM-based methods by large margins while heavily decreasing the model complexity (see Figure 1).

2. Related Works

2.1. Blind Image Super-Resolution

Blind image SR mainly assumes the blur kernel is unknown, which is deemed more applicable in practice. Some methods [1, 25, 37] prioritize individually modelling the blur kernel and perform non-blind SR based on the kernel. KernelGAN [1] explores the internal cross-scale recurrence property of image patches to estimate image-specific blur kernels. MANet [25] focuses on the locality of degradations and presents to estimate spatial variant kernels from tiny LR image patches. Luo *et al.* [28] reformulate the classical degradation model and utilize a deep constrained least squares on the estimated kernel to generate clean features. There are also some methods that investigate the interactions between kernel estimation and SR reconstruction in a single network. IKC [15] and DAN [27] propose to alternately estimate the blur kernel and SR result conditioned on each other in deep unfolding networks. Fu *et al.* [13] propose KXNet which also achieves such a alternate optimization based on the physical generation mechanism between blur kernel and HR image. BSRGAN [49] and RealESRGAN [40] construct synthetic training datasets under more complex degradation models to mimic diverse degradations in real images.

2.2. Diffusion Models

Diffusion model (DM) is derived in [35], which aims to reverse the noising schedule iteratively to generate desired samples. From the arising of DDPM [17], DMs have garnered widespread acclaim as generative models and achieved impressive capabilities in various image restora-

tion tasks. SRDiff [23] and SR3 [33] utilize conditional DMs to tackle SISR problem, surpassing previous GAN-based baselines [39]. Rombach *et al.* [32] propose latent diffusion models (LDM) operating on learned latent space to pursue efficient and effective image synthesis. Kawar *et al.* [20] firstly employ pre-trained DDPMs as learned generative prior to solve multiple linear inverse problems including SISR. Chung *et al.* [5] impose a manifold constraint gradient term put together with the score function to ensure the sampling iterations fall into the manifold. This method is further extended to general noisy inverse problems in [7] with the approximation of posterior sampling. Apart from these non-bind diffusion solvers, GDP [12] generalizes DDPM to image enhancement and blind restoration using a blind degradation estimation strategy. It still remains a challenge to overcome complicated degradations for blind SR. A closely related method to this work is BlindDPS [6] for blind image deblurring, which utilizes two pre-trained DDPMs to provide data and kernel priors and constructs parallel reverse paths to simultaneously restore the kernel and image. Unlike BlindDPS, our method only requires one well-trained DM to learn the two priors and enables alternate optimization for kernel estimation and SR reconstruction in a single reverse process. Besides, based on designed MCFormer, our method can save considerable model parameters while ensuring plausible textures.

3. Preliminary

Diffusion models (DM) [17, 35], or called denoising probabilistic diffusion models (DDPM), are families of generative models, which comprise a diffusion process and a reverse process. Given a clean image \mathbf{x}_0 , the diffusion process defines a Markov chain $\mathbf{x}_{0:T}$ that gradually adds noise to $\mathbf{x}_0 \sim q(\mathbf{x}_0)$ with a fixed variance schedule β_1, \dots, β_T

$$q(\mathbf{x}_t|\mathbf{x}_{t-1}) = \mathcal{N}(\mathbf{x}_t; \sqrt{1 - \beta_t}\mathbf{x}_{t-1}, \beta_t\mathbf{I}) \quad (2)$$

where $\mathbf{x}_T \in \mathcal{N}(0, \mathbf{I})$. Thanks to the property of Markov chain, we can directly acquire \mathbf{x}_t from \mathbf{x}_0 with one forward process $q(\mathbf{x}_t|\mathbf{x}_0) = \mathcal{N}(\mathbf{x}_t; \sqrt{\bar{\alpha}_t}\mathbf{x}_0, (1 - \bar{\alpha}_t)\mathbf{I})$, where $\alpha_t = 1 - \beta_t$ and $\bar{\alpha}_t = \prod_{i=0}^t \alpha_i$.

In the reverse process, there is an opposite parameterized Markov chain $\mathbf{x}_{T:0}$, which starts with a random Gaussian noise $\mathbf{x}_T \in \mathcal{N}(0, \mathbf{I})$ and gradually samples from noised data until reaching \mathbf{x}_0

$$p_\theta(\mathbf{x}_{t-1}|\mathbf{x}_t) = \mathcal{N}(\mathbf{x}_{t-1}; \mu_\theta(\mathbf{x}_t, t), \sigma_\theta^2(\mathbf{x}_t, t)\mathbf{I}) \quad (3)$$

where $\sigma_\theta^2(\mathbf{x}_t, t) = \frac{1 - \bar{\alpha}_{t-1}}{1 - \bar{\alpha}_t} \beta_t$ denotes the variance set to a time-dependent constant. The mean $\mu_\theta(\mathbf{x}_t, t) = \frac{1}{\sqrt{\alpha_t}}(\mathbf{x}_t - \frac{\beta_t}{\sqrt{1 - \bar{\alpha}_t}}\epsilon_\theta(\mathbf{x}_t, t))$ is a learnable parameter estimated by a θ -parameterized denoising network $\epsilon_\theta(\mathbf{x}_t, t)$. Practically, we usually first predict $\tilde{\mathbf{x}}_0$ from \mathbf{x}_t , and sample \mathbf{x}_{t-1} using both

\mathbf{x}_t and $\tilde{\mathbf{x}}_0$ computed as

$$\begin{aligned} \tilde{\mathbf{x}}_0 &= \frac{1}{\sqrt{\alpha_t}}(\mathbf{x}_t - \sqrt{1 - \bar{\alpha}_t}\epsilon_\theta(\mathbf{x}_t, t)) \\ q(\mathbf{x}_{t-1}) &= \mathcal{N}(\mathbf{x}_{t-1}; \mu_t(\mathbf{x}_t, \tilde{\mathbf{x}}_0), \sigma^2\mathbf{I}) \end{aligned} \quad (4)$$

where the model is trained using the simplified objective function $\mathbb{E}_{t, \mathbf{x}_0, \epsilon} [\|\epsilon - \epsilon_\theta(\sqrt{\bar{\alpha}_t}\mathbf{x}_0 + \sqrt{1 - \bar{\alpha}_t}\epsilon, t)\|_2^2]$. Here, $\epsilon \sim \mathcal{N}(0, \mathbf{I})$.

Conditional Diffusion Models aim at generating a target image \mathbf{x}_0 from a diffused noise image $\mathbf{x}_T \sim \mathcal{N}(0, \mathbf{I})$ based on a given condition \mathbf{y} , which train a denoising function $\epsilon_\theta(\mathbf{x}_t, t, \mathbf{y})$ to learn the conditional distribution $p_\theta(\mathbf{x}_t|\mathbf{x}_{t-1}, \mathbf{y})$. Once model trained, one can gradually produce a sequential samples $\mathbf{x}_{T:0}$ for the form $\mathbf{x}_0 \sim p(\mathbf{x}|\mathbf{y})$

$$\mathbf{x}_{t-1} = \frac{1}{\sqrt{\alpha_t}}(\mathbf{x}_t - \frac{\beta_t}{\sqrt{1 - \bar{\alpha}_t}}\epsilon_\theta(\mathbf{x}_t, t, \mathbf{y})) + \sqrt{1 - \bar{\alpha}_t}\epsilon_t \quad (5)$$

where $\epsilon_\theta(\mathbf{x}_t, t, \mathbf{y})$ provides an estimation of the gradient of the data log-density for Langevin dynamics. In this study, we present BlindDiff, which aims to integrate MAP approach and DDPM for blind SR. BlindDiff decomposes the blind SR problem into two subproblems: *i.e.* kernel estimation and HR image restoration, under a MAP framework. The MAP optimizer is further incorporated into DDPM and unfolded along with the reverse process, achieving alternate estimation for blur kernels and HR images. In this section, we will provide theoretical analysis of the proposed method and introduce BindDiff in detail.

3.1. Model Formulation

Given an LR image \mathbf{y} corrupted by the classical degradation model (Eq. (1)), blind SR involves estimating the blur kernel \mathbf{k} and then reconstructing the HR image \mathbf{x} from \mathbf{y} and \mathbf{k} , which can generally formulated as a MAP problem:

$$p(\mathbf{k}, \mathbf{x}|\mathbf{y}) = p(\mathbf{k}|\mathbf{y})p(\mathbf{x}|\mathbf{k}, \mathbf{y}) \quad (6)$$

where \mathbf{k} and \mathbf{x} can be solved by

$$(\mathbf{k}_0, \mathbf{x}_0) = \arg \max_{\mathbf{k}, \mathbf{x}} \log p(\mathbf{k}|\mathbf{y}) + \log p(\mathbf{y}|\mathbf{k}, \mathbf{x}) + \log p(\mathbf{x}) \quad (7)$$

where $\log p(\mathbf{y}|\mathbf{k}, \mathbf{x})$ represents the log-likelihood of \mathbf{y} . $\log p(\mathbf{k}|\mathbf{y})$ denotes the kernel prior captured from \mathbf{y} and $\log p(\mathbf{x})$ refers to the clean image prior that is independent of \mathbf{y} . \mathbf{x}_0 and \mathbf{k}_0 denotes the latent optimal estimation of \mathbf{x} and \mathbf{k} respectively. By decomposing Eq. (7) into two subproblems, we can get

$$\left\{ \begin{aligned} \mathbf{k}_0 &= \arg \max_{\mathbf{k}} \log p(\mathbf{k}|\mathbf{y}) \end{aligned} \right. \quad (8a)$$

$$\left\{ \begin{aligned} \mathbf{x}_0 &= \arg \max_{\mathbf{x}} \log p(\mathbf{y}|\mathbf{k}_0, \mathbf{x}) + \log p(\mathbf{x}) \end{aligned} \right. \quad (8b)$$

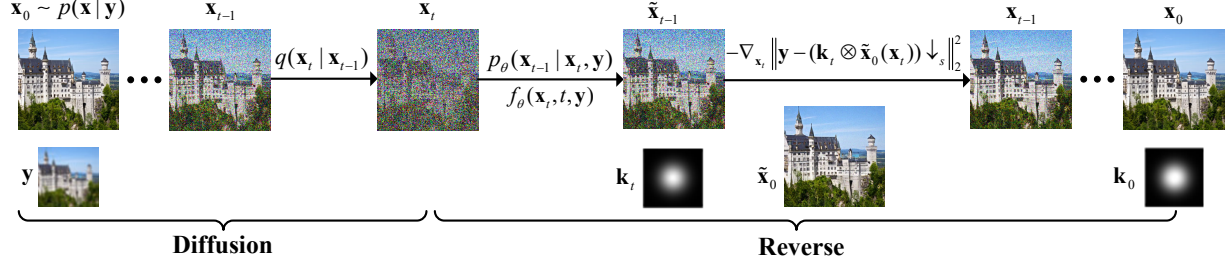


Figure 2. Overview of the forward diffusion process (left→right) that gradually adds Gaussian noise to the original clean image \mathbf{x}_0 . The diffusion model is trained by $f_\theta(\mathbf{x}_t, t, \mathbf{y})$ to provide both kernel and image priors. In the reverse process, for each timestep t , we first sample $\tilde{\mathbf{x}}_{t-1}$ from \mathbf{x}_t and then minimize the residual $\|\mathbf{y} - (\mathbf{k}_t \otimes \tilde{\mathbf{x}}_{t-1})\|_2^2$ with denoised $\tilde{\mathbf{x}}_{t-1}$, leading to \mathbf{x}_{t-1} , where the gradient $\nabla_{\mathbf{x}_t}$ is backpropagated through the whole network.

To make a further step, we can unfold Eq. (8) to form an iterative optimization process

$$\begin{cases} \mathbf{k}_{i-1} = \arg \max_{\mathbf{k}} \log p(\mathbf{k}|\mathbf{y}) \\ \mathbf{x}_i = \arg \max_{\mathbf{x}} \log p(\mathbf{y}|\mathbf{k}_{i-1}, \mathbf{x}) + \log p(\mathbf{x}) \end{cases} \quad (9a) \quad (9b)$$

As we can see, in this formula, the estimation for \mathbf{k} is independent to \mathbf{x} , thus the overall process can be seen as a two-step blind SR pipeline, *i.e.* kernel estimation from \mathbf{y} , and kernel-based non-blind SR. This has been demonstrated to be suboptimal as missing the information from \mathbf{x} for kernel estimation [22, 27]. To address this issue, we follow the common practice in existing end-to-end blind SR methods that incorporate the latent SR image as an auxiliary information to estimate \mathbf{k} . Therefore, Eq. (8a) can be reformulated to

$$\mathbf{k}_{i-1} = \arg \max_{\mathbf{k}} \log p(\mathbf{k}|\mathbf{y}, \mathbf{x}_{i-1}) \quad (10)$$

In addition, since SISR is a conditional image generation task, we often model the condition posterior distribution $p(\mathbf{x}|\mathbf{y})$ as the data prior term rather than $p(\mathbf{x})$. This can be achieved by many well-trained generative models. This work employs DDPMs for that purpose as their excellent generative capabilities.

3.2. Unfolding MAP Approach in DDPM

In the DDPM fashion, we can naturally obtain a sequence denoiser prior $(\tilde{\mathbf{x}}_{T-1}, \dots, \tilde{\mathbf{x}}_t, \dots, \tilde{\mathbf{x}}_0)$ from \mathbf{x}_T by train a conditional model. Here, let's first analyze the solution for \mathbf{x}_0 . With the prior $\tilde{\mathbf{x}}_t$ and LR condition \mathbf{y} , to solve \mathbf{x} , the other key point lies into modelling $\log p(\mathbf{y}|\mathbf{k}, \mathbf{x})$ in the reverse sampling process.

To achieve this, we firstly specify the posterior distribution of this term to be Gaussian: $p(\mathbf{y}|\mathbf{k}, \mathbf{x}) = \mathcal{N}(\mathbf{y}|\mathbf{k} \otimes \mathbf{x}, \sigma^2 \mathbf{I})$. According to the diffusion posterior sampling algorithm [7] for non-blind inverse problems, we modify it to adapt to blind settings, expressed by

$$\log p(\mathbf{y}|\mathbf{k}_t, \mathbf{x}_t) \approx \nabla_{\mathbf{x}_t} \log p(\mathbf{y}|\mathbf{k}_t, \tilde{\mathbf{x}}_0(\mathbf{x}_t)) \quad (11)$$

where $\tilde{\mathbf{x}}_0(\mathbf{x}_t)$ is the denoised sample of \mathbf{x}_t computed by Eq. (4). $\nabla_{\mathbf{x}_t} \log p(\mathbf{y}|\mathbf{k}_t, \tilde{\mathbf{x}}_0(\mathbf{x}_t))$ can be obtained through analytical likelihood for our Gaussian measurement model

$$\nabla_{\mathbf{x}_t} \log p(\mathbf{y}|\mathbf{k}_t, \tilde{\mathbf{x}}_0(\mathbf{x}_t)) = -\frac{1}{\sigma^2} \nabla_{\mathbf{x}_t} \|\mathbf{y} - (\mathbf{k}_t \otimes \tilde{\mathbf{x}}_0(\mathbf{x}_t))\|_2^2 \quad (12)$$

Therefore, we can calculate the gradient $\nabla_{\mathbf{x}_t}$ and backpropagate it through the network to optimize for $p(\mathbf{y}|\mathbf{k}_t, \tilde{\mathbf{x}}_0(\mathbf{x}_t))$, as shown in Figure 2. Noted that, if we convert Eq. (12) into a solution of minimizing the energy function $\mathbf{x}_i = \arg \min_{\mathbf{x}} \frac{1}{2\sigma^2} \|\mathbf{y} - (\mathbf{k}_{i-1} \otimes \mathbf{x})\|_2^2 + \phi(\mathbf{x})$, called **kernel-aware gradient term**, is actually very close to the data fidelity term $\frac{1}{2\sigma^2} \|\mathbf{y} - \mathbf{k}_{i-1} \otimes \mathbf{x}\|_2^2$ that guarantees the solution to be consistent with the degradation knowledge.

Accordingly, what we need is to provide a data prior \mathbf{x}_t as well as a kernel prior \mathbf{k}_t . Combining Eq. (5) and Eq. (9b), since the estimation for both components relies on \mathbf{y} and previous sample \mathbf{x}_t , we propose to train the denoising network with not only the noise-related objective $\epsilon_\theta(\mathbf{x}_t, t, \mathbf{y})$ but also a kernel-related objective. To this end, a modulated conditional transformer (MCFormer, see Figure 3) is proposed consisting a kernel estimator \mathcal{K} and a kernel-modulated transformer backbone, which is trained $\epsilon_\theta(\mathbf{x}_t, t, \mathbf{y})$ and the L_1 loss between the ground truth kernel \mathbf{k}_{gt} and the estimated \mathbf{k} , formulated by

$$\begin{aligned} f_\theta(\mathbf{x}_0, \mathbf{y}, \epsilon) = & \mathbb{E}_{\mathbf{x}_0, \mathbf{y}, \epsilon} \|\epsilon - \epsilon_\theta(\mathbf{y}, \underbrace{\sqrt{\bar{\alpha}_t} \mathbf{x}_0 + \sqrt{1 - \bar{\alpha}_t} \epsilon}_{\tilde{\mathbf{x}}}, \alpha_t)\|_2^2 \\ & + \|\mathbf{k}_{gt} - \underbrace{\mathcal{K}(\mathbf{y}, \sqrt{\bar{\alpha}_t} \mathbf{x}_0 + \sqrt{1 - \bar{\alpha}_t} \epsilon)}_{\mathbf{k}}\|_1 \end{aligned} \quad (13)$$

where $f_\theta(\mathbf{x}_0, \mathbf{y}, \epsilon)$ denotes the combined total loss and $\tilde{\mathbf{x}}$ is the noisy target image.

Once trained, as illustrated in Figure 2, at each reverse iteration, the model enables denoised HR image generation and kernel estimation. Then, by bridging the adjacent iterations with the gradient term $\nabla_{\mathbf{x}_t} \log p(\mathbf{y}|\mathbf{k}_t, \tilde{\mathbf{x}}_0(\mathbf{x}_t))$

Algorithm 1 BlindDiff — Training a DM $f_\theta(\mathbf{x}_0, \mathbf{y}, \epsilon)$

Input: LR image \mathbf{y} as a condition

- 1: **repeat**
 - 2: $(\mathbf{x}_0, \mathbf{y}) \sim p(\mathbf{x}, \mathbf{y})$
 - 3: $(\mathbf{k}_0, \mathbf{y}) \sim p(\mathbf{k}, \mathbf{y}, \mathbf{x})$
 - 4: $\epsilon \sim \mathcal{N}(\mathbf{0}, \mathbf{I})$
 - 5: $T \sim \text{Uniform}(\{1, \dots, T\})$
 - 6: Take gradient descent step on f_θ
 - 7: $\nabla_\theta(\|\epsilon - \epsilon_\theta(\mathbf{y}, \sqrt{\alpha_t}\mathbf{x}_0 + \sqrt{1 - \alpha_t}\epsilon, \alpha_t)\|_2^2) + \|\mathbf{k}_{gt} - \mathcal{K}(\mathbf{y}, \sqrt{\alpha_t}\mathbf{x}_0 + \sqrt{1 - \alpha_t}\epsilon)\|_1$
 - 8: **until** converged
-

Algorithm 2 BlindDiff — Inference in T iterations

Input: LR image \mathbf{y} as a condition, a constant λ

- 1: $(\mathbf{y}|\mathbf{k}, \mathbf{x}) \sim \mathcal{N}(\mathbf{y}|\mathbf{k} \otimes \mathbf{x}, \sigma^2 \mathbf{I})$
 - 2: $\mathbf{x}_T \sim \mathcal{N}(\mathbf{0}, \mathbf{I})$
 - 3: **for** $t = T, \dots, 1$ **do**
 - 4: $\epsilon \sim \mathcal{N}(\mathbf{0}, \mathbf{I})$ if $t > 1$, else $\epsilon = \mathbf{0}$
 - 5: $\tilde{\mathbf{x}}_{t-1} = \frac{1}{\sqrt{\alpha_t}}(\mathbf{x}_t - \frac{\beta_t}{\sqrt{1 - \alpha_t}}\epsilon_\theta(\mathbf{x}_t, t, \mathbf{y}))$ & \mathbf{k}_t generated by f_θ
 - 6: $\mathbf{x}_{t-1} = \tilde{\mathbf{x}}_{t-1} - \lambda \nabla_{\mathbf{x}_t} \|\mathbf{y} - \mathbf{k}_t \otimes \tilde{\mathbf{x}}_0(\mathbf{x}_t)\|_2^2$
 - 7: **end for**
 - 8: **return** $\mathbf{x}_0, \mathbf{k}_0$
-

(Eq. (12)), we can form a close loop that estimates the blur kernel and HR images in a mutual learning manner. With the iteration going on, our BlindDiff enables alternate optimization for the two until approaching their best approximations. Correspondingly, Eq. (9) can be further rewritten as follows

$$\begin{cases} \mathbf{k}_t = \arg \max_{\mathbf{k}} \log p(\mathbf{k}|\mathbf{y}, \mathbf{x}_t) \\ \mathbf{x}_{t-1} = \arg \max_{\mathbf{x}} \log p(\mathbf{y}|\mathbf{k}_t, \tilde{\mathbf{x}}_0(\mathbf{x}_t)) + \log p(\mathbf{x}_t|\mathbf{y}) \end{cases} \quad (14a) \quad (14b)$$

In summary, BlindDiff unfolds the MAP approach into DDPMs, which decouples the blind SR problems into two subproblems that can be alternate solved within the reverse process. The algorithm pseudo-codes of the diffusion and reverse processes in BlindDiff are summarized in Algorithm 1 and Algorithm 2. Notably, this work is quite different to BlindDPS [6] that holds $\mathbf{x}_t, \mathbf{k}_t$ are independent and conducts parallel reverse using two independent pre-trained DDPMs to provide kernel and data priors. In Table 5 and Figure 8, we have demonstrate the superiority of our BlindDiff on the image deblurring task.

3.3. Modulated Conditional Transformer

The detailed architecture of our denoising network, *i.e.* modulated conditional transformer (MCFormer), is shown in Figure 3. MCFormer employs a kernel estimator to learn

blur kernels and a multi-scale hierarchical backbone incorporating transformer blocks to model $f_\theta(\mathbf{x}_0, \mathbf{y}, \epsilon)$.

Kernel Estimator. Given an LR input \mathbf{y} , we first up-sample it to the target resolution using bicubic interpolation and concatenate it with the intermediate image \mathbf{x}_t together. The kernel estimator \mathcal{K} is placed at the beginning of MCFormer for the modulation in later stages. Specifically, it goes through four 5×5 convolutional layers with Leaky ReLU activations (LReLU) to encode image features. Then, we conduct global average pooling on the feature maps to form the estimation elements of the blur kernel, in which the dimensionality of the kernel space is further reduced by principle component analysis (PCA) following [15, 47]. The whole estimation process is formulated as

$$\mathbf{k}_t = \mathcal{K}(\mathbf{y} \uparrow_s, \mathbf{x}_t) \quad (15)$$

where \uparrow_s denotes bicubic upsampling with scale factor s and \mathbf{k}_t is the resulted kernel at timestep t .

Kernel-Modulated Transformer Block. MCFormer embeds the kernel and noise time information into transformer blocks to learn degradation-aware feature presentations. There are three components in the transformer block: 1) Modulations for both the 2) Multi-Dconv head Transposed Attention (MDTA) layer and 3) Gated-Dconv Feed-forward Network (GDFN) layer, as sketched in Figure 3 (right). Let $F \in \mathbb{R}^{H \times W \times C}$ be the intermediate input tensor, where H , W , and C denotes the height, width, and channel dimension of F respectively. The time t and \mathbf{k}_t are another two inputs. It is notable that $t \in \mathbb{R}^C$ is already pre-processed by a multi-layer perceptron (MLP) before embedding. Then we leverage another MLP to project \mathbf{k}_t to the same dimension as t . The first modulation module provides affine transformation for F after layer normalization

$$\bar{F} = \mathcal{M}_1(t, \mathbf{k}_t, F) = \gamma_1 \odot \text{Norm}(F) + \tau_1 \quad (16)$$

where \mathcal{M}_1 denotes the transformation function. γ_1 and τ_1 are learnable parameters by two linear layers after fusing t and \mathbf{k}_t , which serve as a scaling and shifting operations respectively. \bar{F} is the modulated feature. Then, we apply MDTA on \bar{F} for global connectivity modelling as it has been demonstrated to be an efficient yet effective attention mechanism [46], produced $\tilde{F} \in \mathbb{R}^{H \times W \times C}$.

After that, another modulation module is adopted to operate on the attentive feature

$$\hat{F} = \mathcal{M}_2(t, \mathbf{k}_t, \tilde{F}) = \gamma_2 \odot \tilde{F} + \tau_2 \quad (17)$$

where γ_2 and τ_2 also learned from the fused feature of t and \mathbf{k}_t . A GDFN [46] is finally utilized to aggregate local features and mine meaningful information from spatially neighbouring pixel positions, resulting output feature $F' \in \mathbb{R}^{H \times W \times C}$ which is expected to be more discriminative and robust to various degradations.

Table 1. $4\times$ SR quantitative comparison on datasets with *Gaussian8* kernels. **Bold**: Best, underline: second best.

Method	Set5		BSD100		DIV2K100			FFHQ			ImageNet-1K		
	LPIPS↓	PSNR↑	LPIPS↓	PSNR↑	LPIPS↓	FID↓	PSNR↑	LPIPS↓	FID↓	PSNR↑	LPIPS↓	FID↓	PSNR↑
IKC [15]	0.2459	31.67	0.3699	27.37	0.3047	64.44	28.45	0.2443	51.73	32.01	0.2702	48.62	29.06
DAN [27]	0.2321	31.90	0.3603	27.51	0.2933	59.76	<u>28.91</u>	0.2167	45.33	<u>32.80</u>	0.2615	<u>47.81</u>	<u>29.54</u>
AdaTarget [18]	0.2351	31.58	0.3598	27.43	0.2919	57.72	28.80	0.2362	48.19	32.24	0.2631	56.81	29.40
BSRGAN [49]	0.3175	27.50	0.3752	25.32	0.3371	85.47	25.47	0.2435	40.22	28.80	0.3390	73.20	26.16
DCLS [28]	<u>0.2284</u>	32.12	<u>0.3574</u>	27.60	<u>0.2855</u>	<u>57.57</u>	29.04	<u>0.2147</u>	45.02	32.86	0.2580	47.83	29.65
KDSR [43]	0.2440	<u>32.11</u>	0.3759	27.64	0.3125	72.34	28.76	0.2543	53.10	32.29	0.2801	53.15	29.43
DiffPIR [53]	0.3398	26.51	0.4470	24.96	0.4131	94.00	25.11	0.2795	44.81	28.08	0.3747	62.70	25.77
GT kernel+DPS [7]	—	—	—	—	—	—	—	0.3059	<u>33.77</u>	24.69	0.4521	64.87	22.13
GDP [12]	0.4089	25.15	0.5132	23.94	0.4765	80.41	23.88	0.3731	80.39	26.70	<u>0.4331</u>	82.85	24.49
BlindDiff (ours)	0.2147	30.17	0.3099	26.34	0.2588	34.15	26.83	0.1754	22.02	30.87	0.2411	37.18	28.12

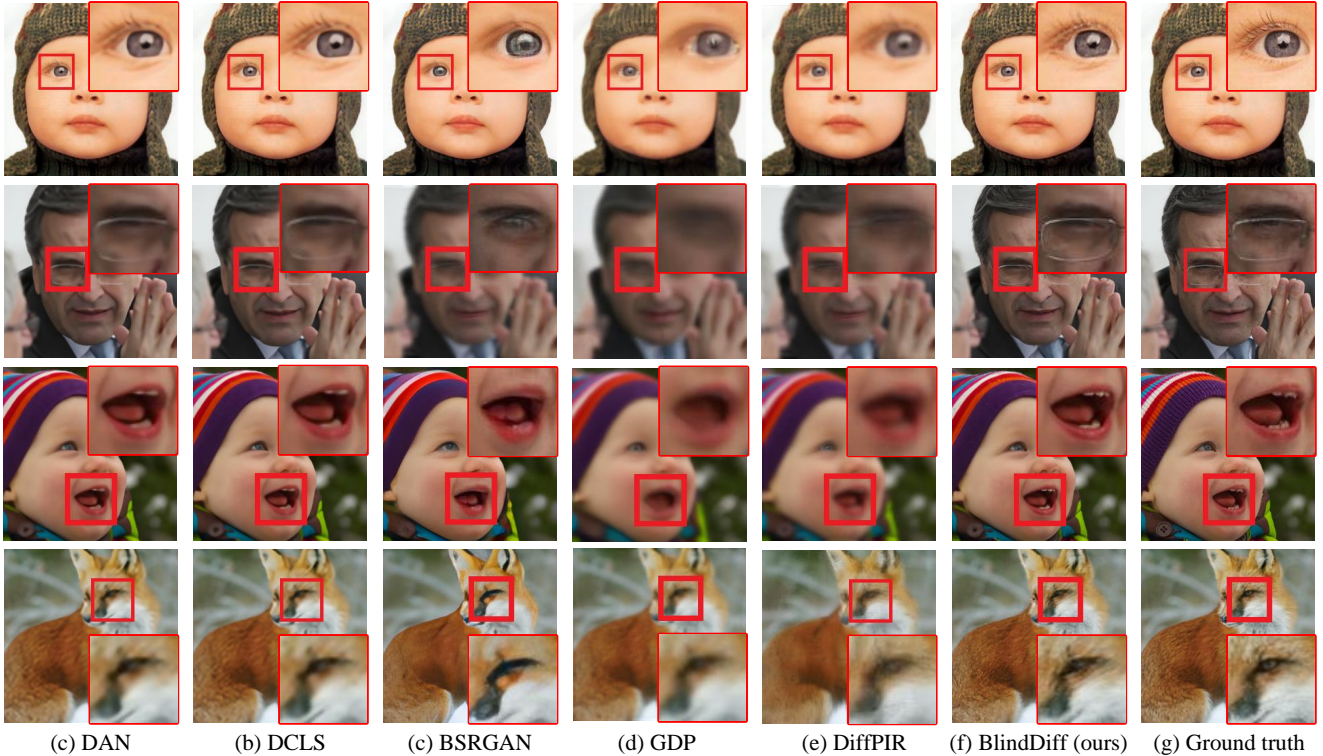


Figure 4. Visual comparisons of $4\times$ blind SR methods on isotropic Gaussian kernels.

recent state-of-the-art methods including 6 CNN-based blind SR methods: IKC [15], DAN [27], AdaTarget [18], DCLS [28], BSRGAN [49], KDSR [43] and 3 DM-based SR methods: DPS [7], GDP [12], DiffPIR [53]. All the methods are evaluated on Set5, BSD100, DIV2K100, FFHQ, and ImageNet-1K datasets, which are synthesized by *Gaussian8*. Here, considering the limitation of existing DM methods for tackling arbitrary resolutions (*i.e.* Set5), we apply the patch-based strategy in GDP [12] with adaptive instance normalization to obtain more natural SR results. Due to the heavy computation cost of DPS (out of memory), we only report its performance on FFHQ and ImageNet-1K. As shown in Table 1, BlindDiff generally

outperforms all the methods in terms of FID and LPIPS on all datasets while also surpassing DM methods in terms of all the 3 metrics by large margins. Specifically, BlindDiff exceeds BSRGAN by 0.09 LPIPS and 36 FID on ImageNet-1K even though it trained for complicated degradations with paired training data. DiffPIR suffers from severe performance drops when directly applied to blind degraded images. DPS performs better than DiffPIR when GT kernels are available, but still exhibits worse perceptual quality and pixel faithfulness than ours. Surprisingly, although GDP adopts a degradation-guidance strategy to tackle blind degradation, the results indicate it is not well applicable to blind SR. Figure 4 visualize the $4\times$ SR results on face and

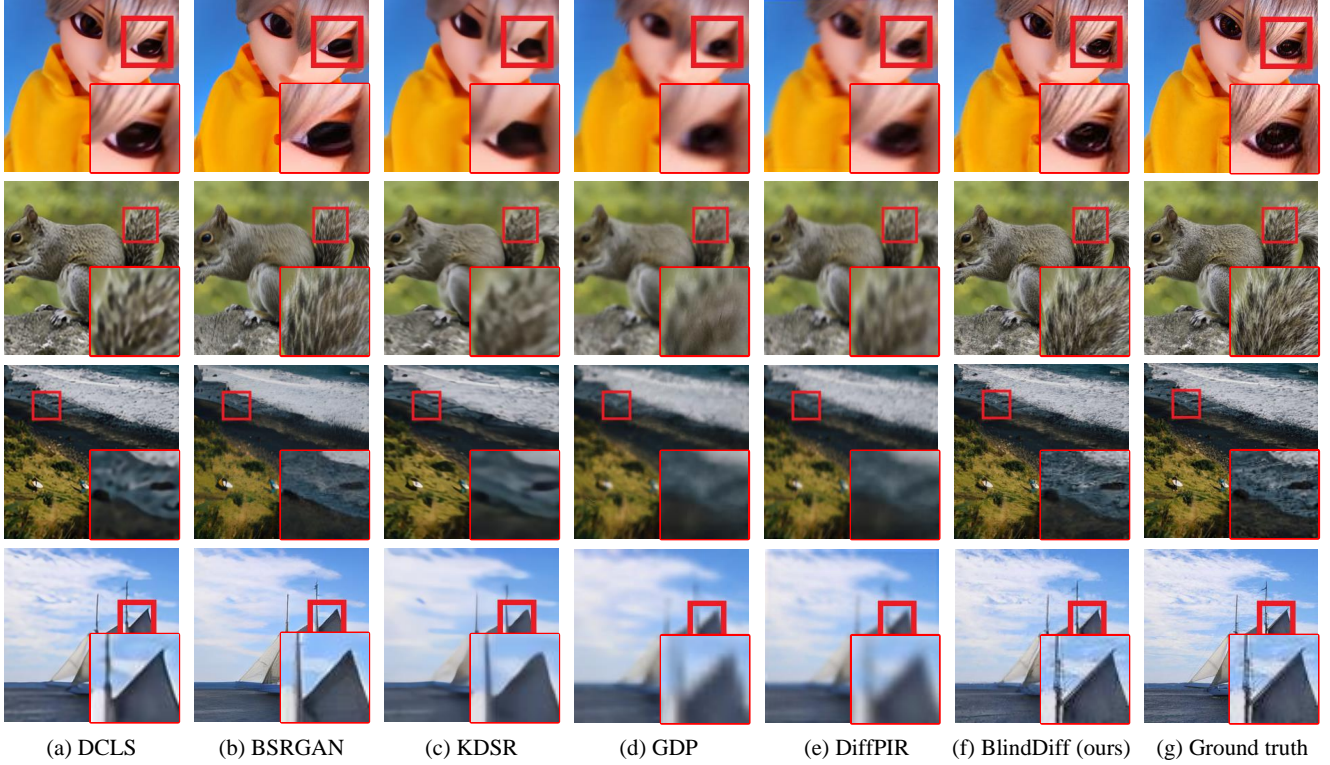


Figure 5. Visual comparisons of $4\times$ blind SR methods on anisotropic Gaussian kernels.

Table 2. $4\times$ SR quantitative comparison on datasets with random anisotropic Gaussian kernels. **Bold**: Best, underline: second best.

Method	DIV2K100			ImageNet-1K		
	LPIPS↓	FID↓	PSNR↑	LPIPS↓	FID↓	PSNR↑
DASR [38]	0.4476	149.11	25.46	0.4116	100.66	26.22
DAN [27]	0.3597	96.63	26.74	0.3272	68.52	27.33
DCLS [28]	0.3085	69.98	28.31	<u>0.2791</u>	<u>54.59</u>	29.02
BSRGAN [49]	0.3526	98.39	24.90	0.3546	80.95	25.60
AdaTarget [18]	<u>0.2923</u>	77.04	28.25	0.3249	56.81	27.58
DARSR [52]	0.4956	148.34	24.05	0.4618	107.79	24.22
KDSR [43]	0.4328	144.25	25.82	0.4035	101.22	26.48
DiffPIR [53]	0.4387	113.02	24.75	0.4049	76.18	25.31
GT kernel + DPS [7]	—	—	—	0.4550	63.47	21.99
GDP [12]	0.4868	137.99	23.63	0.4491	90.49	24.16
BlindDiff (ours)	0.2763	42.85	26.32	0.2571	42.62	27.53

natural images. It is obvious that the SR results of BlindDiff are much clearer and reveal more details.

Evaluation with Anisotropic Gaussian Blur Kernels.

We evaluate our BlindDiff on DIV2K100 and ImageNet-1K datasets, where the HR images are degraded by random anisotropic Gaussian kernels. We compare BlindDiff with 7 CNN methods: DASR [38], DAN [27], DCLS [28], BSRGAN [49], AdaTarget [18], DARSR [52], KDSR [43] and 3 DM methods: DiffPIR [53], DPS [7], GDP [12]. Quantitative results are illustrated in Table 2 and the model complexity measured by parameters and Multi-Adds are shown in Figure 1. Clearly, even in this more general and challenging case, BlindDiff still outperforms other methods. Com-

pared to the most SOTA CNN method DCLS, BlindDiff obtains 38.8% and 21.9% FID improvements on DIV2K100 and ImageNet-1K respectively. Furthermore, BlindDiff surpasses the best DM method “GT Kernel+DPS” by 20.85 in terms of FID while only consuming about 5% parameters (26.51M v.s. 552.81M, Figure 1(a)) and 1% computations (Figure 1(b)). In addition, the visual comparison of these methods is provided in Figure 5. As we can see, the SR images of BlindDiff have more realistic textures, fewer blurs, and sharper boundaries than compared methods.

Evaluation on Real-World Images. We also investigate the effectiveness of BlindDiff for real-world degradations by conducting experiments on several real-world images from RealSR [3] and RealSRSet [49] datasets, which contains unknown blurs, noise or compression artifacts. The $4\times$ SR results are shown in Figure 6. We can observe that DAN, DCLS, and DiffPIR tend to generate blurs. Though BSRGAN can effectively remove the noise and blurs, it is easier to produce the SR images with over-smooth textures, leading to details loss. In contrast, our method can recover clearer details and more natural textures.

4.4. Ablation Study

In this section, we verify the effectiveness of each component in BlindDiff. For efficient comparison, all the models are pre-trained for 100K iterations and tested on Set5.

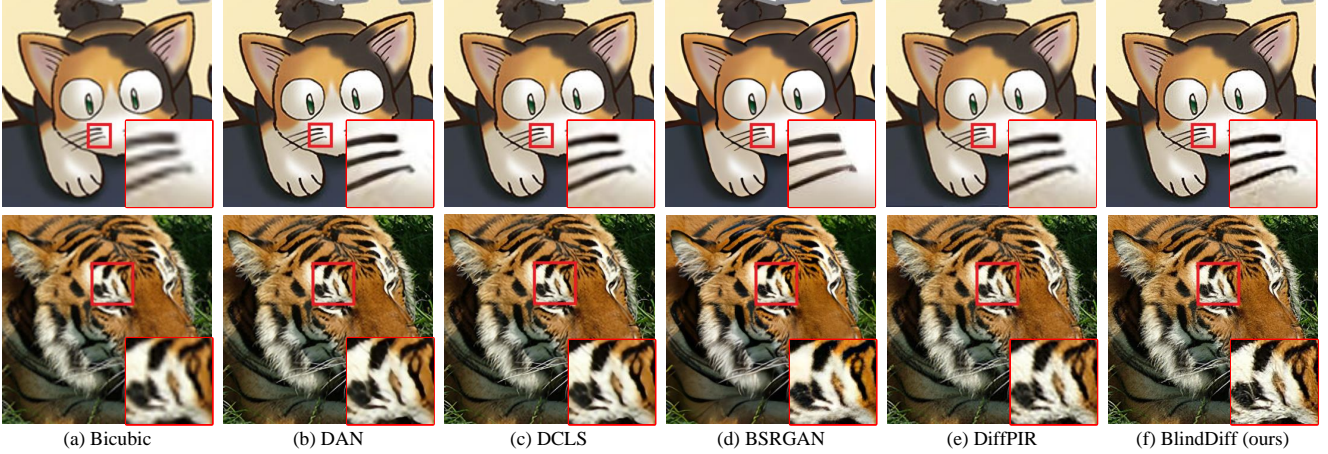


Figure 6. Visual results of $4\times$ blind SR methods on RealSRSet.

Table 3. Investigation of the Proposed Components in BlindDiff. We evaluate the LPIPS performance on Set5 for $4\times$ blind SR.

Variant	Kernel Constraint	Kernel Modulation	Gradient Term		LPIPS↓
			Bicubic-based	Kernel-aware	
Baseline	×	×	×	×	0.2382
Model A	✓	×	✓	×	0.3277
Model B	✓	×	×	✓	0.2300
Model C	✓	✓	×	×	0.2298
Model D	✓	✓	×	✓	0.2289
Model E	✓	✓	✓	×	0.3236
Model F	×	×	✓	×	0.3268

Effect of Kernel Prior. In BlindDiff, we propose the MCFormer trained with noise and kernel constraints (Eq. (13)) to provide additional kernel prior. To investigate its effect, we first construct a **Baseline** model that uses none of our proposed component. As shown in Table 3, when we add the kernel prior but use the bicubic-based gradient term (**Model A**), the model suffers from performance drop due to the difference between the learned kernel and bicubic one. When cooperating with the more related kernel-aware gradient term (**Model B**), the LPIPS is obviously improved. Continuously, by combining it with the kernel modulation operations, leading to **Model C**, compared to the **Baseline**, the result not only proves that effectively utilizing kernel prior knowledge in hidden space is beneficial for better SR reconstruction, but also demonstrates the effectiveness of the modulation operation.

Effect of Kernel-aware Gradient term. The kernel-aware gradient term is the key to achieve alternate kernel and HR image optimization. Firstly, the comparison between **Model A** and **Model B** indicates its superiority for blind blur kernels against the bicubic-based. When we combine it with the kernel constraint and modulation in one model (**Model D**), our BlindDiff can fully exploit the kernel knowledge so that achieves the best LPIPS. To more intuitively illustrate the influence of this component, we replace

Table 4. Impact of the kernel-aware gradient term. We evaluate the LPIPS performance on Set5 for $4\times$ blind SR.

λ	0	0.1	1	5	10
LPIPS	0.2298	0.2296	0.2289	0.2716	0.2899

it with bicubic-based term in **Model D**, resulting in **Model E**, one can see the LPIPS value is heavily decreased. More extremely, we remove all the components but only add the bicubic-based term (**Model F**), the result further indicates the adverse effects of the kernel difference and the necessity of our kernel-aware gradient term.

Balance for Kernel-Aware Gradient Term. As shown in Algorithm 2, in the reverse process, we practically calculate the kernel-aware gradient and backpropagate it with a balance hyperweight λ . Here, we investigate the impact of this term by change the value of λ from 0 to 10, where $\lambda = 0$ means the model without considering such a gradient back-propagation strategy. The detailed experimental results are listed in Table 4. One can see when we increase λ from 0 to 1, the gradient term becomes more important and provides positive impact for better SR image reconstruction. However, when we further increase λ to 10, the model suffers from performance degradation due to the over-emphasizing of the gradient term. These results validate the effectiveness of the proposed kernel-aware gradient term. In our experiments, we accordingly set $\lambda = 1$.

Sampling Step Visualization. Since our BlindDiff involves the alternate optimization for blur kernel and HR image during posterior sampling, here, we visualize the intermediate sampling steps to investigate how the iteration number affects BlindDiff. Here, we calculate the LPIPS and L1 error to measure the estimation accuracy of the SR images and blur kernels at different iterations, where the results are visualized in Figure 7a. One can see that, as the iteration number is larger than 2, BlindDiff almost keep sta-

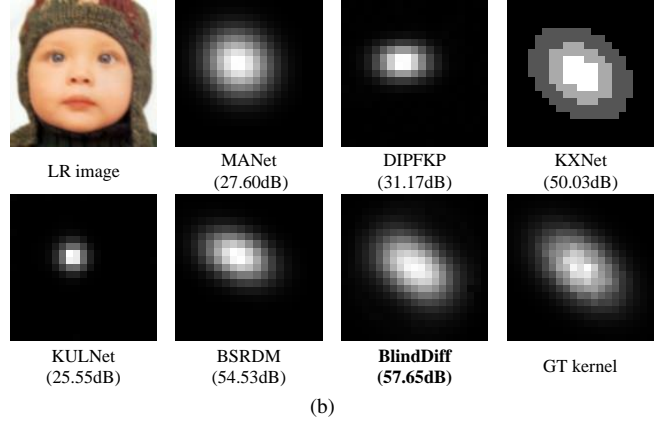
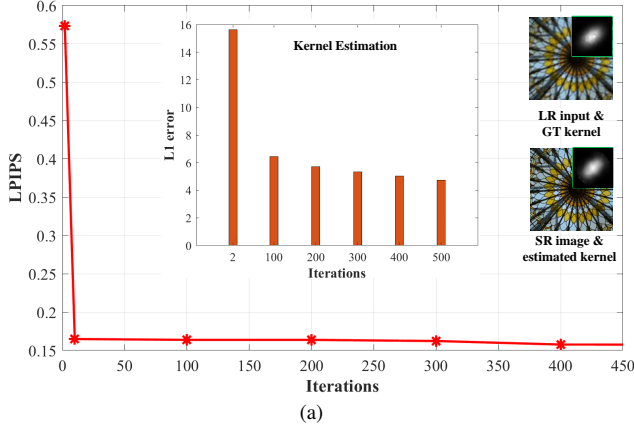


Figure 7. (a) Visualization of the results under different sampling iterations. We report the LPIPS and L1 error to measure the estimation accuracy of the SR images and blur kernels, respectively; (b) Kernel estimation results on “baby” in Set5 degraded by an anisotropic kernel with $\sigma_x = 2.5$ and $\sigma_y = 4.0$.

ble and progressively reaches the upper bound. Besides, we observe that the L1 errors between the predicted kernel and ground truth (GT) kernel also decreases as the iteration goes on, getting closer to the GT kernel. This visualization of the sampling process validates that our BlindDiff can achieve mutually alternate optimization for blur kernel estimation and HR image restoration.

Kernel Estimation. To reveal the kernel estimation ability of BlindDiff, following [25], we calculate the LR image PSNR to quantitatively compare the kernel loss. Here, we synthesize a reference LR image using a GT kernel and a HR image, where an accurate kernel is expected to reconstruct a similar LR image from the same HR one. In Figure 7b, we compare BlindDiff with existing kernel estimation-based blind SR methods including MANet [25], DIPFKP [26], KXNet [13], KULNet [11], and BSRDM [44]. One can see that BlindDiff generates a blur kernel that is more consistent with the GT kernel while other methods produce unreliable results. Besides, equipped with the resulted kernel, BlindDiff can reconstruct a LR image with the best PSNR performance.

Extension to Blind Image Deblurring. To investigate the generalization ability of our method, we conduct experiments on blind deblurring and compared it with several recent state-of-the-art deblurring methods including MPNet [45], Restormer [46], and BlindDPS [6]. Following BlindDPS, motion blur kernel is randomly generated with intensity 0.5 using the code ¹. All the methods are evaluated on FFHQ datasets, where the quantitative and qualitative results are shown in Table 5 and Figure 8. As we can see, our BlindDiff not only achieves the best pixel perceptual quality (LPIPS/FID) and faithfulness (PSNR), but also restore the images with more plausible textures.

Method	FFHQ (256 × 256)		
	LPIPS ↓	FID ↓	PSNR ↑
MPNet [45]	0.5706	185.58	21.12
Restormer [46]	0.5050	160.87	22.36
BlindDPS [6]	<u>0.2842</u>	<u>30.06</u>	<u>24.03</u>
BlindDiff (ours)	0.2542	29.90	26.80

Table 5. Quantitative comparison for blind deblurring on FFHQ for blind deblurring. **Bold**: Best, underline: second best.

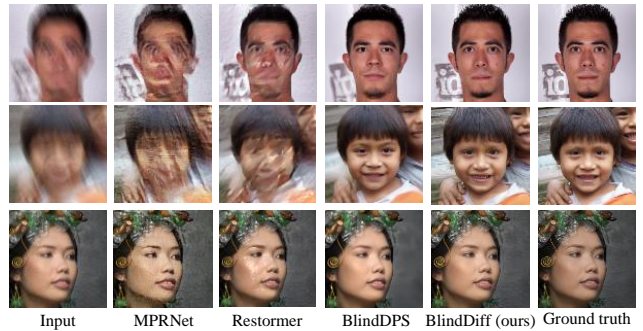


Figure 8. Visual comparison for blind deblurring.

5. Conclusion

In this work, we propose BlindDiff, a DM-based super-resolver that integrates MAP approach into DMs seamlessly to tackle the blind SR problem. Our BlindDiff constructs a distinctive reverse pipeline that unfolds the MAP approach along with the reverse process, enabling alternate optimization for joint blur kernel estimation and HR image recovery. We theoretically analyze the methodology of such a MAP-driven DDPM for blind SR. We present a modulated conditional transformer and make it allows to provide generative kernel and image priors by introducing an kernel

¹<https://github.com/LeviBorodenko/motionblur>

estimation objective to train with the noise prediction objective together. With extensive experiments, we show that BlindDiff establishes state-of-the-art performance.

References

- [1] Sefi Bell-Kligler, Assaf Shocher, and Michal Irani. Blind super-resolution kernel estimation using an internal-gan. In *NeurIPS*, 2019. 1, 2
- [2] Marco Bevilacqua, Aline Roumy, Christine Guillemot, and Marie-Line Alberi Morel. Low-complexity single-image super-resolution based on non-negative neighbour embedding. In *BMVC*, pages 135.1–135.10, 2012. 6
- [3] Jianrui Cai, Hui Zeng, Hongwei Yong, Zisheng Cao, and Lei Zhang. Toward real-world single image super-resolution: A new benchmark and a new model. In *ICCV*, pages 3086–3095, 2019. 8
- [4] Xiangyu Chen, Xintao Wang, Jiantao Zhou, Yu Qiao, and Chao Dong. Activating more pixels in image super-resolution transformer. In *CVPR*, pages 22367–22377, 2023. 1
- [5] Hyungjin Chung, Byeongsu Sim, Dohoon Ryu, and Jong Chul Ye. Improving diffusion models for inverse problems using manifold constraints. In *NeurIPS*, 2022. 2, 3
- [6] Hyungjin Chung, Jeongsol Kim, Sehui Kim, and Jong Chul Ye. Parallel diffusion models of operator and image for blind inverse problems. In *CVPR*, pages 6059–6069, 2023. 3, 5, 10
- [7] Hyungjin Chung, Jeongsol Kim, Michael Thompson McCann, Marc Louis Klasky, and Jong Chul Ye. Diffusion posterior sampling for general noisy inverse problems. In *ICLR*, 2023. 2, 3, 4, 7, 8
- [8] Jia Deng, Wei Dong, Richard Socher, Li-Jia Li, Kai Li, and Li Fei-Fei. Imagenet: A large-scale hierarchical image database. *PAMI*, 43(12):4217–4228, 2015. 6
- [9] Chao Dong, Chen Change Loy, Kaiming He, and Xiaoou Tang. Image super-resolution using deep convolutional networks. *PAMI*, 38(2):295–307, 2015. 1
- [10] Wan-Cyuan Fan, Yen-Chun Chen, Dongdong Chen, Yu Cheng, Lu Yuan, and Yu-Chiang Frank Wang. Frido: Feature pyramid diffusion for complex scene image synthesis. In *AAAI*, pages 579–587, 2023. 2
- [11] Zhenxuan Fang, Weisheng Dong, Xin Li, Jinjian Wu, Leida Li, and Guangming Shi. Uncertainty learning in kernel estimation for multi-stage blind image super-resolution. In *ECCV*, pages 144–161, 2022. 10
- [12] Ben Fei, Zhaoyang Lyu, Liang Pan, Junzhe Zhang, Weidong Yang, Tianyue Luo, Bo Zhang, and Bo Dai. Generative diffusion prior for unified image restoration and enhancement. In *CVPR*, pages 9935–9946, 2023. 3, 7, 8
- [13] Jiahong Fu, Hong Wang, Qi Xie, Qian Zhao, Deyu Meng, and Zongben Xu. Kxnet: A model-driven deep neural network for blind super-resolution. In *ECCV*, pages 235–253, 2022. 1, 2, 10
- [14] Guangwei Gao, Wenjie Li, Juncheng Li, Fei Wu, Huimin Lu, and Yi Yu. Feature distillation interaction weighting network for lightweight image super-resolution. In *AAAI*, pages 661–669, 2022. 1
- [15] Jinjin Gu, Hannan Lu, Wangmeng Zuo, and Chao Dong. Blind super-resolution with iterative kernel correction. In *CVPR*, pages 1604–1613, 2019. 1, 2, 5, 7
- [16] Martin Heusel, Hubert Ramsauer, and Thomas Unterthiner. Gans trained by a two time-scale update rule converge to a local nash equilibrium. In *NeurIPS*, 2017. 6
- [17] Jonathan Ho, Ajay Jain, and Pieter Abbeel. Denoising diffusion probabilistic models. In *NeurIPS*, 2020. 2, 3
- [18] Younghyun Jo, Seoung Wug Oh, Peter Vajda, and Seon Joo Kim. Tackling the ill-posedness of super-resolution through adaptive target generation. In *CVPR*, pages 16236–16245, 2021. 7, 8
- [19] Tero Karras, Samuli Laine, and Timo Aila. A style-based generator architecture for generative adversarial networks. In *CVPR*, pages 4401–4410, 2019. 6
- [20] Bahjat Kawar, Michael Elad, Stefano Ermon, and Jiaming Song. Denoising diffusion restoration models. In *ICLRW*, 2022. 2, 3
- [21] Diederik P. Kingma and Ba Jimmy. Adam: A method for stochastic optimization. In *ICLR*, 2015. 6
- [22] Feng Li, Yixuan Wu, Huihui Bai, Weisi Lin, Runmin Cong, and Yao Zhao. Learning detail-structure alternative optimization for blind super-resolution. *TMM*, 25:2825–2838, 2023. 1, 4
- [23] Haoying Li, Yifan Yang, Meng Chang, Shiqi Chen, Huajun Feng, Zhihai Xu, Qi Li, and Yueting Chen. Srdiff: Single image super-resolution with diffusion probabilistic models. *Neurocomputing*, 479:47–59, 2022. 2, 3
- [24] Jingyun Liang, Jiezhang Cao, Guolei Sun, Kai Zhang, Luc Van Gool, and Radu Timofte. Swinir: Image restoration using swin transformer. In *ICCVW*, pages 1833–1844, 2021. 1
- [25] Jingyun Liang, Guolei Sun, Kai Zhang, Luc Van Gool, and Radu Timofte. Mutual affine network for spatially variant kernel estimation in blind image super-resolution. In *ICCV*, pages 4076–4085, 2021. 1, 2, 10
- [26] Jingyun Liang, Kai Zhang, Shuhang Gu, Luc Van Gool, and Radu Timofte. Flow-based kernel prior with application to blind super-resolution. In *CVPR*, pages 10601–10610, 2021. 10
- [27] Zhengxiong Luo, Yan Huang, Shang Li, Liang Wang, and Tieniu Tan. Unfolding the alternating optimization for blind super-resolution. In *NeurIPS*, 2020. 1, 2, 4, 6, 7, 8
- [28] Ziwei Luo, Haibin Huang, Lei Yu, Youwei Li, Haoqiang Fan, and Shuaicheng Liu. Deep constrained least squares for blind image super-resolution. In *CVPR*, pages 17642–17652, 2022. 2, 7, 8
- [29] David Martin, Charless Fowlkes, Jitendra Malik, and Doron Tal. A database of human segmented natural images and its application to evaluating segmentation algorithms and measuring ecological statistics. In *ICCV*, page 416, 2001. 6
- [30] David Martin, Charless Fowlkes, Jitendra Malik, and Doron Tal. Ntire 2017 challenge on single image super-resolution: Methods and results. In *CVPRW*, pages 1110–1121, 2017. 6

- [31] Aditya Ramesh, Prafulla Dhariwal, Alex Nichol, Casey Chu, and Mark Chen. Hierarchical text-conditional image generation with clip latents. *arXiv: 2204.06125*, 2022. [2](#)
- [32] Robin Rombach, Andreas Blattmann, Dominik Lorenz, Patrick Esser, and Björn Ommer. High-resolution image synthesis with latent diffusion models. In *CVPR*, pages 10674–10685, 2022. [2](#), [3](#)
- [33] Chitwan Saharia, Jonathan Ho, William Chan, Tim Salimans, David J Fleet, and Mohammad Norouzi. Image super-resolution via iterative refinement. *PAMI*, 45(04):4713–4726, 2023. [2](#), [3](#)
- [34] Assaf Shocher, Nadav Cohen, and Michal Irani. “zero-shot” super-resolution using deep internal learning. In *CVPR*, pages 3118–3126, 2018. [1](#)
- [35] Jascha Sohl-Dickstein, Eric Weiss, Niru Maheswaranathan, and Surya Ganguli. Deep unsupervised learning using nonequilibrium thermodynamics. In *ICML*, pages 2256–2265, 2015. [2](#), [3](#)
- [36] Yang Song, Jascha Sohl-Dickstein, Diederik P. Kingma, Abhishek Kumar, Stefano Ermon, and Ben Poole. Score-based generative modeling through stochastic differential equations. In *ICLR*, 2021. [2](#)
- [37] Guangpin Tao, Xiaozhong Ji, Wenzhuo Wang, Shuo Chen, Chuming Lin, Yun Cao, Tong Lu, Donghao Luo, and Ying Tai. Spectrum-to-kernel translation for accurate blind image super-resolution. In *NeurIPS*, 2021. [2](#)
- [38] Longguang Wang, Yingqian Wang, Xiaoyu Dong, Qingyu Xu, Jungang Yang, Wei An, and Yulan Guo. Unsupervised degradation representation learning for blind super-resolution. In *CVPR*, pages 10581–10590, 2021. [1](#), [8](#)
- [39] Xintao Wang, Ke Yu, Shixiang Wu, Jinjin Gu, Yihao Liu, Chao Dong, Chen Change Loy, Yu Qiao, and Xiaoou Tang. Esrgan: Enhanced super-resolution generative adversarial networks. In *ECCVW*, pages 63–79, 2018. [1](#), [3](#)
- [40] Xintao Wang, Liangbin Xie, Chao Dong, and Ying Shan. Real-esrgan: Training real-world blind super-resolution with pure synthetic data. In *ICCVW*, pages 1905–1914, 2021. [2](#)
- [41] Yinhuai Wang, Jiwen Yu, and Jian Zhang. Zero-shot image restoration using denoising diffusion null-space model. In *ICML*, 2022. [2](#)
- [42] Jie Wu, Runmin Cong, Leyuan Fang, Chunle Guo, Bob Zhang, and Pedram Ghamisi. Unpaired remote sensing image super-resolution with content-preserving weak supervision neural network. *Sci. China Inf. Sci.*, 66(1):119105:1–119105:2, 2023. [1](#)
- [43] Bin Xia, Yulun Zhang, Yitong Wang, Yapeng Tian, Wenming Yang, Radu Timofte, and Luc Van Gool. Kernel distillation based degradation estimation for blind super-resolution. In *ICLR*, 2023. [7](#), [8](#)
- [44] zhongheng Yue, Qian Zhao, Jianwen Xie, Lei Zhang, and Kwan-Yee K. Meng, Deyu amd Wong. Blind image super-resolution with elaborate degradation modeling on noise and kernel. In *CVPR*, pages 2128–2138, 2022. [10](#)
- [45] Syed Waqas Zamir, Aditya Arora, Salman Khan, Munawar Hayat, Fahad Shahbaz Khan, Ming-Hsuan Yang, and Shao Ling. Multi-stage progressive image restoration. In *CVPR*, pages 14816–14826, 2021. [10](#)
- [46] Syed Waqas Zamir, Aditya Arora, Salman Khan, Munawar Hayat, Fahad Shahbaz Khan, and Ming-Hsuan Yang. Restormer: Efficient transformer for high-resolution image restoration. In *CVPR*, pages 5728–5739, 2022. [5](#), [10](#)
- [47] Kai Zhang, Wangmeng Zuo, and Zhang Lei. Learning a single convolutional super-resolution network for multiple degradations. In *CVPR*, pages 3262–3271, 2018. [5](#)
- [48] Kai Zhang, Luc Van Gool, and Radu Timofte. Deep unfolding network for image super-resolution. In *CVPR*, pages 3217–3226, 2020. [1](#)
- [49] Kai Zhang, Jingyun Liang, Luc Van Gool, and Radu Timofte. Designing a practical degradation model for deep blind image super-resolution. In *ICCV*, pages 4771–4780, 2021. [2](#), [7](#), [8](#)
- [50] Richard Zhang, Phillip Isola, Alexei A Efros, Eli Shechtman, and Oliver Wang. The unreasonable effectiveness of deep features as a perceptual metric. In *CVPR*, pages 586–595, 2018. [6](#)
- [51] Yulun Zhang, Kunpeng Li, Kai Li, Lichen Wang, Bineng Zhong, and Yun Fu. Image super-resolution using very deep residual channel attention networks. In *ECCV*, pages 294–310, 2018. [1](#)
- [52] Hongyang Zhou, Xiaobin Zhu, Jianqing Zhu, Zheng Han, Shi-Xue Zhang, Jingyan Qin, and Xu-Cheng Yin. Learning correction filter via degradation-adaptive regression for blind single image super-resolution. In *ICCV*, pages 12365–12375, 2023. [8](#)
- [53] Yuanzhi Zhu, Kai Zhang, Jingyun Liang, Jiezhong Cao, Bihan Wen, Radu Timofte, and Luc Van Gool. Denoising diffusion models for plug-and-play image restoration. In *CVPRW*, pages 1219–1229, 2023. [7](#), [8](#)